



An improvised method for the synthesis of ZnAl₂O₄/ZnO nanocomposite and its use as a photocatalyst

Zaki Eldin Ali Abdalla¹ · Mukesh Kumar² · Ismail Hassan¹ · Firdous Ahmad Ahangar¹ · Wael Saud Althubaiti²

Received: 29 March 2018 / Accepted: 17 September 2018 / Published online: 8 October 2018
© Springer Science+Business Media, LLC, part of Springer Nature 2018

Abstract

Nanocomposite material ZnAl₂O₄/ZnO was prepared via layered double hydroxides co-precipitation method in the presence of triblock copolymer, Pluronic F127 as the template with different concentrations at pH 7. The material was characterized by XRD, N₂ adsorption/desorption, UV–Vis diffused reflectance, TGA–DTA and SEM. XRD and SEM results reveal that ZnAl₂O₄/ZnO was highly ordered nanocrystalline material. N₂ adsorption/desorption studies indicate that the pore size and pore volume increased significantly with the increase in concentration of F127 copolymer template, while the surface area is slightly decreased with increase of F127 template. TGA–DTA results reveal that the thermal stability of material increased after adding F127 template. The material was tested for its photocatalytic activity for a solution containing methyl orange dye and the 95.6% decolorization was achieved within 1 h. The intensive absorption light observed by UV–Vis reflectance of the catalyst confirmed high activity of the catalyst and suggest the probable photocatalytic degradation mechanism.

1 Introduction

During current times much attention has been focused on heterogeneous photocatalysis because it is one of the strategies that adopt to solve environmental pollution [1]. Photocatalysis has focused on the use of semiconductor materials as photocatalysts for the complete destruction of organic, inorganic, and microbial pollutants, under ambient pressure and temperature [2, 3]. ZnO has been extensively used in photocatalytic processes because it has many attractive properties such as chemical and physical stability, environmentally friendly, low cost, and powerful oxidation strength [4]. In spite of these properties, there are many drawbacks limit the wide application of ZnO in this process such as its wide band gap 3.20 eV and low quantum efficiency [5, 6]. To improve the photocatalytic activity of ZnO, one or more semiconductors with matching band potentials are combined with ZnO, therefore a coupling of the ZnO and ZnAl₂O₄ has

been used, because the coupling of the bandgap structure of the nanocomposites ensured the efficient separation of photogenerated e⁻ and h⁺ pairs, which is important for the enhanced photocatalytic performance compared with single phase ZnO material [7–10]. Zinc aluminate (ZnAl₂O₄), a member of the spinel family of complexes, has been extensively employed in the synthesis of functional ceramic materials due to its superior catalytic, thermal and optical properties [11]. The formation of ZnAl₂O₄ spinels has been obtained by different routes, such as solid-state reaction [12], sol–gel [13], co-precipitation [14], polymeric precursor [15], modified citrate [16], hydrothermal [17], and microwave-hydrothermal [18]. Another attempt to synthesize spinels is use of layered double hydroxides (LDHs) as a precursor which has proved to be an effective way for the preparation of mixed metal oxides [19]. LDHs are a class of synthetic anionic clays that consist of positively charged layers containing alternatively distributed divalent and trivalent cations in the sheets and charge balancing anions between the layers [20, 21]. LDHs can be represented by the general formula [M^{II}_{1-x}M^{III}_x(OH)₂]^{x+}(Aⁿ⁻)_{x/n}·yH₂O, where M^{II} (e.g. Mg²⁺, Zn²⁺, Ni²⁺) and M^{III} (e.g. Al³⁺, Fe³⁺, Cr³⁺) cations occupy octahedral holes in a brucite-like layer and Aⁿ⁻ anion is located in the hydrated interlayer galleries. The positive charge of the host lattice is neutralized by the intercalated anions in the interlayers, and its remaining space is occupied by water molecules. M^{II}–M^{III} LDH can intercalate

✉ Zaki Eldin Ali Abdalla
z.aliabdalla@psau.edu.sa

¹ Department of Chemistry, College of Arts and Science, Prince Sattam Bin Abdulaziz University, P.O. Box 56, Wadi Al-Dawasir 11991, Saudi Arabia

² Department of Electrical Engineering, College of Engineering, Prince Sattam Bin Abdulaziz University, P.O. Box 54, Wadi Al-Dawasir 11991, Saudi Arabia

various types of inorganic anions such as NO_3^- , F^- , SO_4^{2-} , CO_3^{2-} and organic anions, such as phenols, anionic surfactant templates. The identities of the divalent and trivalent cations (M^{II} and M^{III} , respectively) and the interlayer anion ($\text{A}^{\text{n-}}$), together with the value of the stoichiometric coefficient (x), may be varied over a wide range, giving rise to a large class of isostructural materials [22–25]. Considered generally as promising materials LDH is an excellent precursor for preparing pure spinels because the x is adjustable and all metal cations distribute uniformly at an atomic level in the lamella of LDH [26]. Liu et al. prepared high crystalline ZnAl_2O_4 spinel via $[\text{ZnAl}_2(\text{OH})_6]\text{CO}_3 \cdot n\text{H}_2\text{O}$ by urea hydrolysis method [25]. The brucite-like layers can be stacked in different ways leading to different structures by using a template. Templates such as vesicles, micelles, micro emulsions, peptides, and polymers have been reported and direct the formation of the target material with specific size, morphology and properties [27]. In order to prepare LDHs which are more suitable with most hydrophobic polymers, an LDHs with newly designed LDHs which has a modified surface is required for the preparation of LDH based polymer [28–30]. A great variety of layered nanocomposites can be prepared from the combination between polymers and layered inorganic solids. Compared to unmodified polymers, the resulting materials present dramatic improvement in properties such as rigidity, chemical and mechanical resistance, and density, impermeability to gases, thermal stability, electrical and thermal conductivity, as well as high degree of optical transparency [31–33]. Some reports [34, 35] of earlier works for preparation of mixed metal oxides using organic templates such as polystyrene and cellulose form highly ordered mesoporous material after removal of organic matrix. Organic dyes which are widely used in textile and food industries represent an important source of environmental contamination. Most of the dyes are toxic to aquatic creatures and have carcinogenic effects on humans [36, 37]. Photocatalytic techniques using metal semiconductors, such as ZnO , TiO_2 , SnO_2 or CdS , have been widely applied for the degradation of the organic pollutants in aqueous solutions [38–41]. The photocatalytic degradation of organic dyes can be carried out using LDH either as such or in calcined form. The $\text{ZnO}/\text{Zn}-\text{Al}$ LDH nanostructures were also calcined to fabricate $\text{ZnO}/\text{ZnAl}_2\text{O}_4$ nanospheres as photocatalysts [42, 43] and they found that in many studies calcination of LDH material improved photocatalytic activity by the formation of mixed metal oxide nanocrystals [44–46]. In this work we prepare ZnAl mixed metal oxide via LDH co-precipitation method by using sodium aluminate to hydrolyze it into sodium hydroxide and metal hydroxides by smooth transition of pH in the presence of a non-ionic surfactant, Pluronic F127 poly(ethylene oxide)–poly(propylene oxide)–poly(ethylene oxide) (PEO–PPO–PEO) block copolymer as the template in order to decrease the agglomeration

rate and achieve uniform particle size. Then we studied its catalytic activity in photo-degradation of methyl orange dye.

2 Experimental

2.1 Synthesis of catalyst

ZnAl mixed metal oxide were synthesized via LDHs using the co-precipitation method at pH 7 with $\text{Zn}:\text{Al}$ ratios = 2 and in the presence and absence of copolymer F127 as surfactant, as follows; 50 mmol of zinc acetate ($\text{Zn}(\text{CH}_3\text{COO})_2 \cdot 2\text{H}_2\text{O}$) was dissolved in 75 mL water and 50 mL of ethanol and then added different amounts of Pluronic F127 i.e. 0.0, 0.25 and 0.5 mmol to this solution. To this mixture, 25 mmol sodium aluminate in 50 mL water was added drop wise from burette under stirring. Then the resultant white precipitate was transferred to 250 mL Teflon lined stainless steel for hydrothermal synthesis at 100 °C in an oven for 24 h. All samples were subsequently allowed to cool to room temperature. Then they were filtered, and dried at 80 °C for 24 h. The white powders obtained were calcined at 550 °C for 6 h. The solids were designated as $\text{ZnAl}0.00$, $\text{ZnAl}0.25$, and $\text{ZnAl}0.50$ where the digits indicate the amount of F-127 copolymer surfactant added in the preparation of material.

2.2 Characterization techniques

The crystal phase and structure of materials was analyzed by PXRD using Rigaku ultima with $\text{Cu K}\alpha$ refraction, $\lambda = 1.5418 \text{ \AA}$ at 40 kV. Brunauer–Emmett–Teller (BET) was used to analyze the surface area using Micro Active for TriStar II plus Version 2.03. The pore size and pore volume distribution were calculated by Barrett–Joyner–Halenda (BJH). UV–Vis diffused reflectance a spectrum was obtained using a UV–Vis spectrophotometer (JASCO, V-670). The morphology of the samples has been done by using Quanta FEG 250 scanning electron microscope and the elemental analysis of all samples was performed by scanning electron microscope using secondary electron (SE) at an accelerating voltage of 20 kV, and the attached energy dispersive X-ray spectrometer (EDS, Oxford Inc.) was employed as a detector for subsequent elemental composition analysis. Perkin Elmer diamond TG/DTA analyzer was used to carry out the thermogravimetric analysis experiments and dried alumina powder was used as reference material for taking the hectograms. Samples were heated from ambient temperature to 800 °C in nitrogen atmosphere at a flow rate of 20 mL/min.

2.3 Photocatalytic activity

Decolorization of the methyl orange dye solution experiments were conducted under the UV Sterilization tube 2×8 W, with wavelength 254 nm. The experiments were performed in a closed dark wooden chamber ($50 \text{ cm} \times 35 \text{ cm} \times 40 \text{ cm}$) to avoid interference from ambient lights at room temperature. The UV lamps were horizontally installed inside the UV chamber. In the photocatalytic studies, irradiation was carried out in 0.5 L plastic bowl reactor (dimension 15 cm) containing 0.05 L of methyl orange dye solution. The reactor was placed at the center of the chamber, under the UV lamps at a distance of 15 cm. 10 mg/L of methyl orange dye solution was prepared by dissolving the appropriate amount of dye powder in distilled water. 50 mL of this solution was placed in the plastic bowl reactor followed by the addition of the catalyst. Then the mixture was subjected to irradiation from UV lamps by placing on magnetic stirrer. In all conditions, the aqueous dye solutions were magnetically stirred well at 400 rpm. During UV irradiation, the sample solutions were taken from the photo reactor at a particular interval of time until clear solution was obtained.

The samples were centrifuged to separate the catalyst for measuring the absorbance of the solutions. The change of methyl orange dye concentration in the photoreactor was determined quantitatively by measuring absorbance using UV–Vis spectrophotometer (Jasco V-730 UV–Visible/NIR Spectrophotometer). Calibration curves (linear, $R^2 = 0.999$) of the dye solution were constructed from standard methyl orange dye solution at various concentrations.

3 Results and discussion

The reaction pathways for the synthesis of ZnAl mixed oxide via LDH co-precipitation and calcination are shown in Scheme 1.

3.1 Catalyst characterization

The PXRD for calcined and uncalcined material is represented in Fig. 1 for Zn–Al materials in the presence and absence of copolymer F-127. The XRD patterns of as prepared ZnAl-LDH samples display diffraction peaks between

Scheme 1 Synthesis of $\text{ZnAl}_2\text{O}_4/\text{ZnO}$

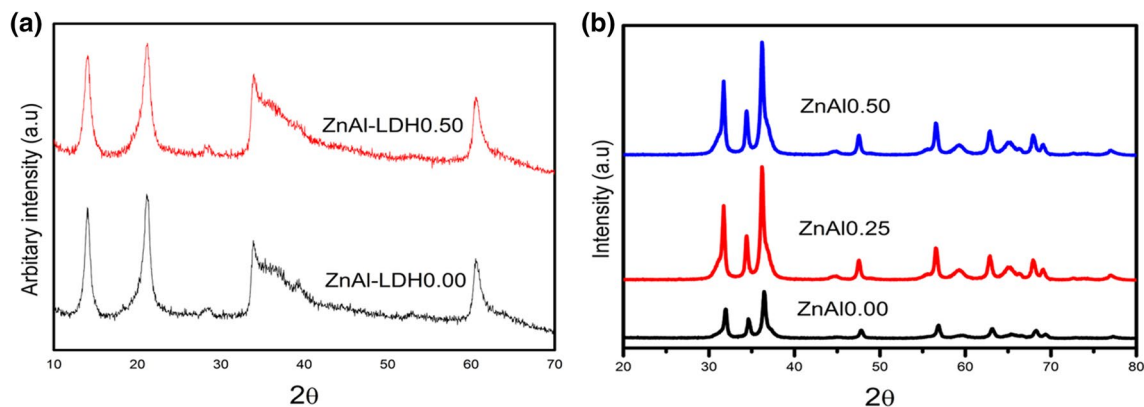
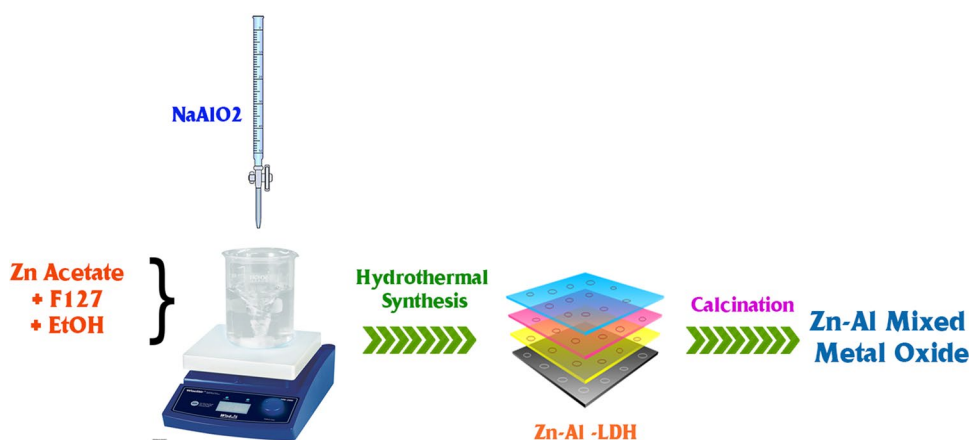


Fig. 1 XRD of **a** uncalcined samples, **b** calcined samples

2θ 13.8° and 60.5° angles indexed as 003, 006, 009, 110 and the peaks 009 reflection overlaps with 018 resulting in a broad signal planes. All of these diffraction peaks signify the hydrothermalite-type materials. Figure 1b shows the PXRD analysis of calcined ZnAl0.00, ZnAl0.25, ZnAl0.50 at 550°C . From the figure we can observe that the diffraction peaks at 31.59° , 34.18° , 36.12° , 47.44° , 56.50° , 62.65° and 68.07° reflect the structure of ZnO but with slightly higher than that of pure ZnO. In addition to ZnO diffraction peak, we can observe the diffraction peaks of ZnAl_2O_4 at higher 2θ angles 44.69° , 59.09° , 65.07° and 77.04° [9, 10]. The presence of zinc aluminate diffraction peaks and the slightly shifted peaks of ZnO represent the incorporation of zinc aluminate into the ZnO framework resulting in the formation of $\text{ZnAl}_2\text{O}_4/\text{ZnO}$ nanocomposite material with high crystallinity through the calcination of ZnAl-LDH at 550°C . Figure 2 shows type IV in the classification of IUPAC, characteristic of a solid mesoporous material. The Isotherms of

ZnAl0.00 without F127 exhibit a H1-type hysteresis loop, which is caused by capillary condensation and is characteristic feature of layered materials. While the ZnAl0.25 and ZnAl0.50 with F127 showed a H3-type hysteresis loop, which was attributed to the presence of slit type pores that are coming from the plate-like particles. This kind of hysteresis is typical for the presence of open large pores, which allow easy diffusion of the reactants through the materials [41]. Table 1 display the values of the BET specific surface areas, pore size and pore volumes. It shows that on increasing the amount of F-127 there is slight decrease in surface area while the pore volume and pore size are increased. The decrease in surface area may be because of their pores block due to presence of carbon residue. The corresponding pore size distribution (PSD) curves in Fig. 2 represent broad mesopore size distribution, however, with increasing amount of F127, the sample exhibits sharper and larger PSD. Larger pore size of catalysts is advantageous as it makes

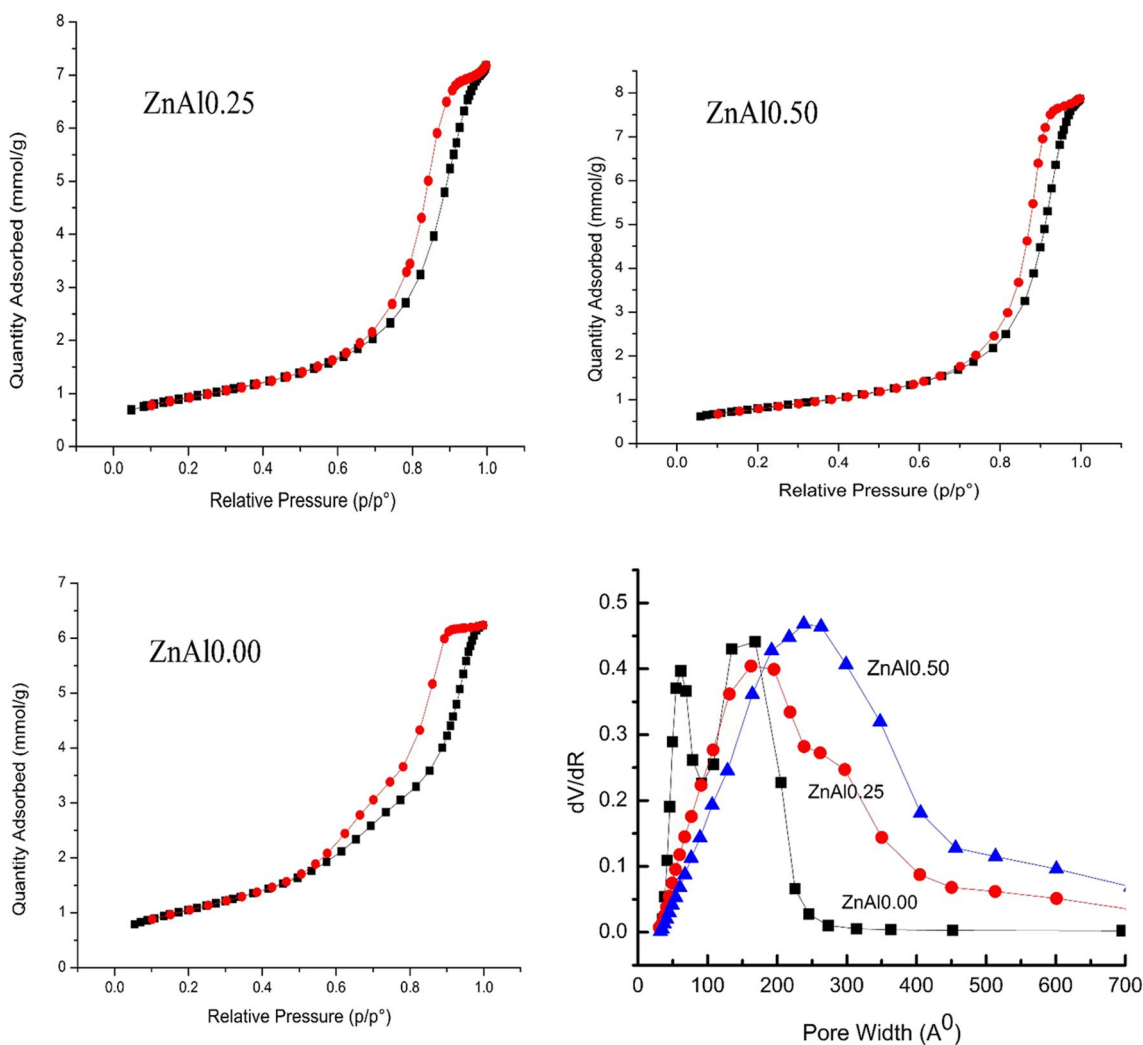
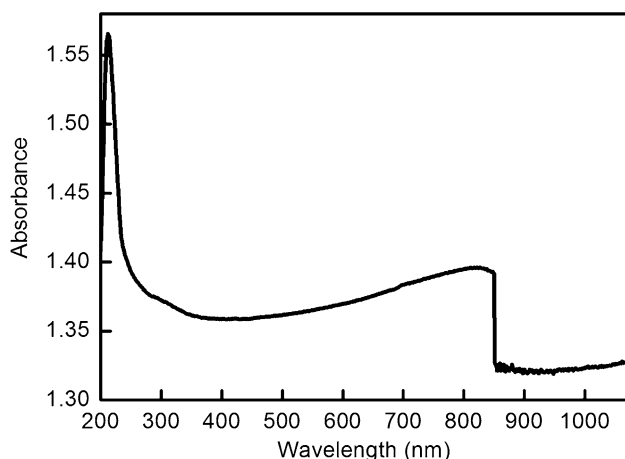


Fig. 2 N_2 adsorption/desorption isotherms and PSD curves

Table 1 Texture parameters for ZnAl₂O₄/ZnO nanocomposite

Samples	wt% Zn	wt% Al	Zn/Al mole ratio	Surface area (m ² /g)	Pore volume (cm ³ /g)	Pore size (Å)
ZnAl0.00	44.21	10.92	1.68	85.59	0.24	84.50
ZnAl0.25	52.50	11.55	1.88	74.45	0.27	110.02
ZnAl0.50	50.44	11.41	1.82	64.03	0.29	139.69

**Fig. 3** UV–Vis diffuse reflectance absorption of ZnAl0.50

the transport of reactants more efficient and, therefore, such catalysts could be more active in the catalytic reaction. From the figures it is observed that on changing the amount of F127 the pore size exhibits sharper and larger PSD. The UV–Vis diffuse reflectance absorption of ZnAl0.50 (Fig. 3) displays a sharp absorption peak at wavelength 215 nm in UV region and also there is intense absorption in the visible region, which could indicate that the nanocomposites is highly active for photocatalytic in visible-light irradiation. The peak centered at 800 nm, may be due to the doping of carbon resulted from F127 template, which was not totally removed during calcination which may cause the decrease of the surface area as increasing the amount of the F127 template [10]. Figure 4 elucidates the morphology of the uncalcined and the calcined samples as shown. It can be seen that the ZnAl-LDH precursor has hexagonal shape which transforms into smaller crystallites after calcination. ZnAl0.50 has average shape size 50 nm; while it is uncalcined ZnAl-LDH precursor has average size 75 nm. Also we can observe that the material prepared ZnAl0.00 in the absence of F127 united particles like cluster shape. In Fig. 5 the EDS pattern confirm the average amount of Zn/Al ratio is approximately equal to value of 2.0 as used in the starting solutions which contains both zinc and aluminum as represented in Table 1. The TG–DTA curve of a synthesized ZnAl0.00 and ZnAl0.25 are shown in Fig. 6 and Table 1. A synthesized ZnAl0.00 and ZnAl0.25 exhibits four mass-loss

endothermic stages in TG curves. The endothermic peaks at 85 °C correspond to the removal of physisorbed water while the peak around 225 °C due to removal of interlayer water. The last two peaks at 340–438 °C resulted from dehydroxylation of the layers and the decomposition of the interlayer anions, however, the final stage of the degradation shifted to the right in the synthesized ZnAl0.25 from 426 to 438 °C. This may be due to the presence of F127 which coats the material and results in higher stability.

3.2 Decolorization of MO dye solution

The UV irradiation resulting in decolorization of MO dye solutions carried out in the absence and presence of the catalysts as a function of irradiation time is deduced. Efficiency of the decolorization system at irradiation time was calculated by following equation.

$$\text{Decolorization Efficiency (\%)} = \frac{C_0 - C_t}{C_0}$$

where C_0 (mg/L) and C_t (mg/L) represent the concentration of dye solution for the initial and at time t , respectively, of the test sample. From the equation, the decolorization efficiency (%) indicates percentage of the net concentration change. Blank experiments performed without the catalyst under identical UV irradiation for 60 min showed no significant change in concentration of MO. The results show dye decomposition in presence of catalyst/irradiation and the decolorization efficiency of the MO solutions increased with irradiation time. The effect of the copolymer F-127 used as a surfactant in the preparation of the catalyst for the decolorization efficiency of MO dye solution in Fig. 7 results reveal that the decolorization efficiency increased with increase of F-127 surfactant used in the catalyst preparation. For example, the catalyst ZnAl0.50 had a higher decolorization efficiency 71.50% in 5 min. while ZnAl0.25 and ZnAl0.00 had decolorization efficiency of 66.70%, 56.70% respectively under same conditions. The large pore size factor of the catalyst helps in the transport of reactants more efficiently and, therefore, such catalysts could be more active in the catalytic reaction. Moreover, the surface area has no significant effect compared to the pore size. Similar observations can be made at a time of 90 min. where the efficiency has increased from 91.9 to 95.6 on increasing amount of

Fig. 4 SEM images of **a, b** ZnAl_{0.00}, **c, d** ZnAl-LDH_{0.50}, **e, f** ZnAl_{0.50}

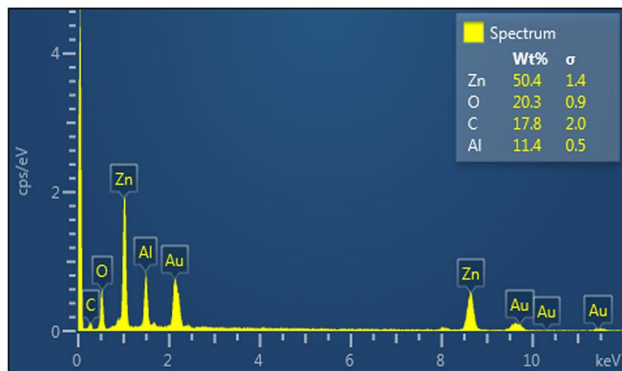
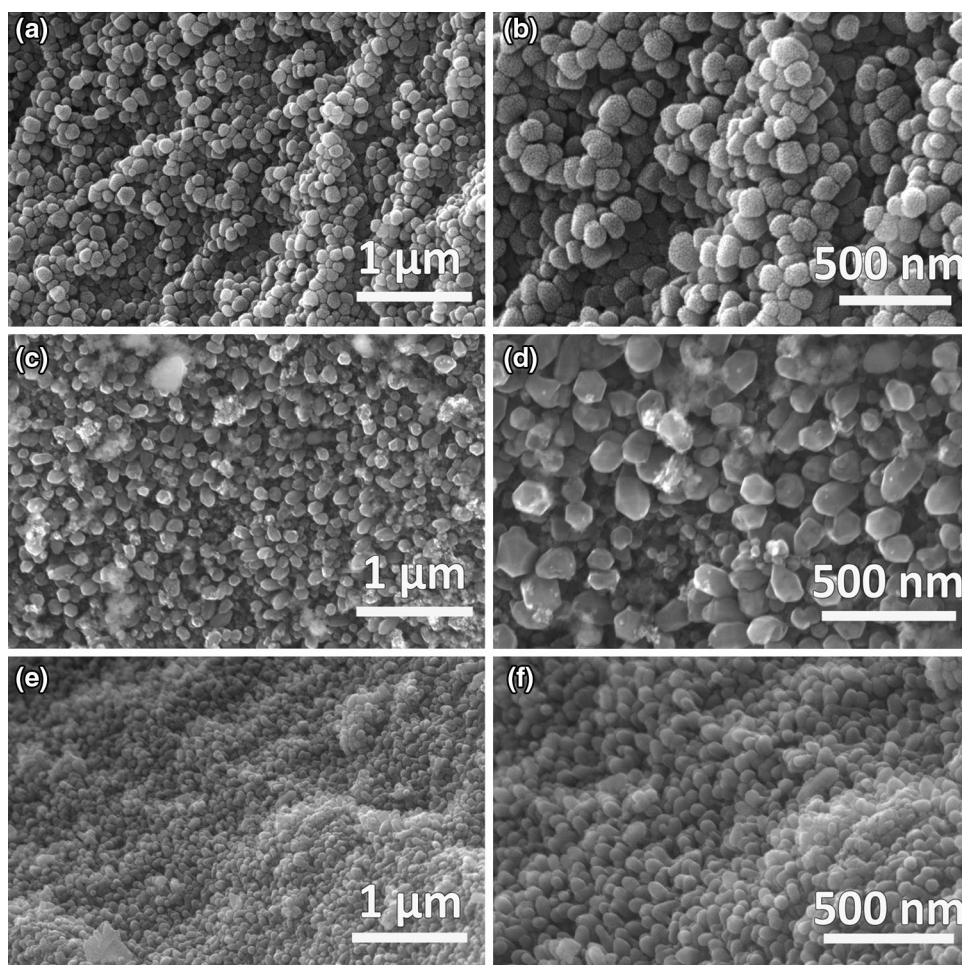


Fig. 5 EDS spectrum of ZnAl_{0.50}

F127 under same conditions. Figure 8 shows the absorption spectra changes of MO dye solutions during the photocatalytic process by the ZnAl_{0.50} catalysts. The characteristic peaks of the MO dyes showed absorption at 464 nm. The decrease of absorption peak means that the double bond of the chromophore in the dye structure had been destroyed after irradiation with the ZnAl_{0.50} catalyst. The peak

became gradually smoother with increasing irradiation time, which means that sufficient photocatalytic reaction had been gained to destroy the chromophore of the dyes. The effects of ZnAl_{0.50} catalyst concentrations on photocatalytic decolorization efficiency were also studied with two concentrations 0.1 g/L and 0.05 g/L as a function of irradiation time. Figure 9 shows the photocatalytic decolorization of MO dye in aqueous solution. The decolorization efficiency (%) at different amount of 0.05 g ZnAl_{0.50}/L catalyst was lower than that of the ZnAl_{0.50} amount at 0.1 g ZnAl_{0.50}/L. The increase in concentration resulted in decrease in the time required for decolorization of methyl orange. This was because of the increase in the number of active sites on the photocatalyst surface. It can be found from the table that at time $t = 1$ min the amount of dye decomposed is 12.9% for 0.05 g catalyst while it is 37.6% for 0.1 g of the catalyst. Further at $t = 10$ min it is 64.5% for 0.05 g catalyst while it is 78.1% for 0.1 g of the catalyst. The decomposition is almost complete at 60 min as the amount of dye decomposed is 91.7% for 0.05 g of F127 and 95.5% for 0.1 g of the catalyst. Based on above results and referred to previous works [9, 10, 47] a possible mechanism for the degradation of methyl

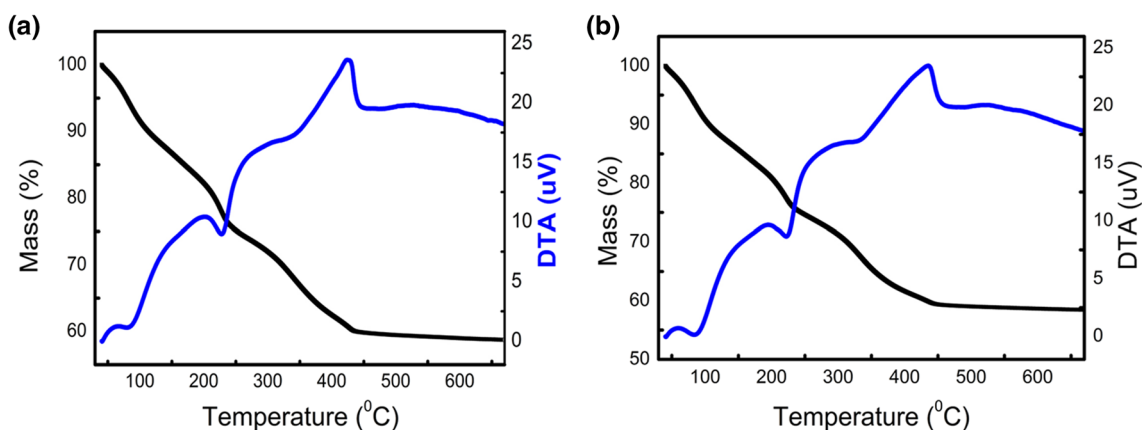


Fig. 6 TGA–DTA curves of **a** ZnAl0.00 and **b** ZnAl0.25

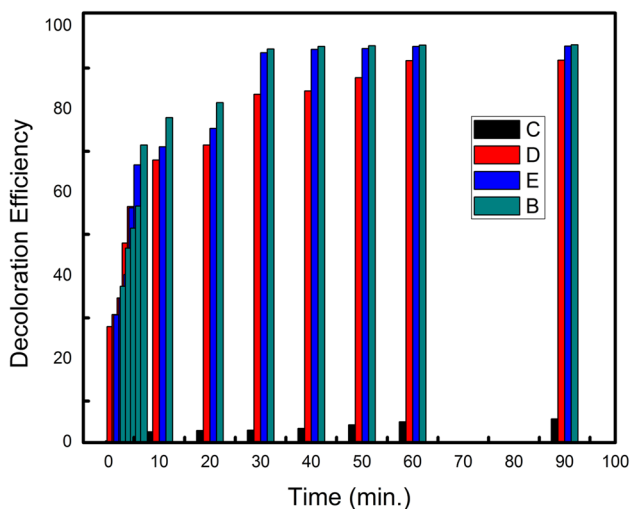


Fig. 7 MO decolorization efficiency versus irradiation time by the catalyst (b) ZnAl0.50 (e) ZnAl0.25 (d) ZnAl0.00 (c) in the absence of catalyst

orange is supposed that ZnAl₂O₄ and ZnO in ZnAl₂O₄/ZnO catalyst are coupled together and their conduction band (CB) and valence band (VB) levels will have a good matching. The energy gap between corresponding band levels drives the e⁻ and h⁺ pairs from one particle to its neighbors to form a spatial separation. Such process is energetically favorable which photogenerated e⁻ and h⁺ pairs. The resulted O₂⁻ and OH⁻ be will oxidized by photogenerated holes (h⁺) to generate the free radicals ·O₂⁻ and ·OH which are responsible the degradation of methyl orange.

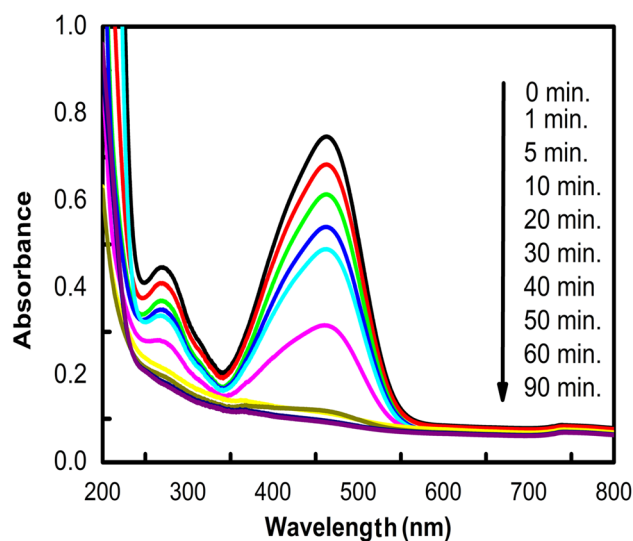


Fig. 8 UV–Vis absorption spectra of MO after different irradiation times using ZnAl0.50 as a photocatalyst

4 Conclusion

In summary, we synthesized ZnAl₂O₄/ZnO, nanocomposite material via LDHs co-precipitation method in the presence of F127 copolymer as the template with different concentrations at pH 7. The characterization techniques revealed that the ZnAl₂O₄/ZnO was highly ordered nanocrystalline material and the pore size and pore volume increased significantly with the increase in concentration of F127. This feature exhibits potential for increase in catalytic properties, thus providing a chance to utilize them in decolorization of a solution containing methyl orange dyes and has scope in the management of waste waters.

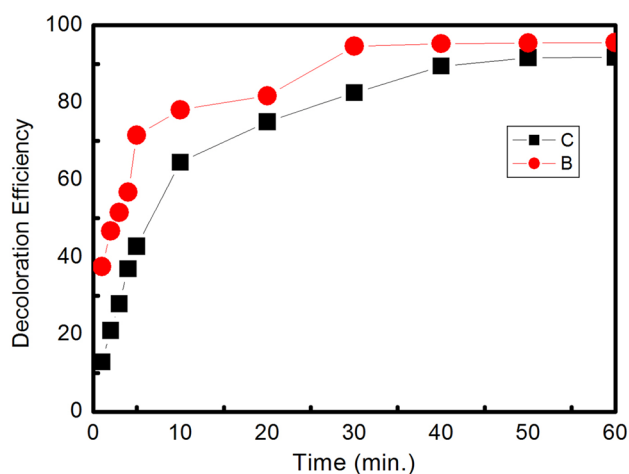


Fig. 9 MO decolorization efficiency versus irradiation time by different amount of ZnAl_{0.50} catalyst with two concentrations (b) 0.05 g ZnAl_{0.50}/L and (c) 0.1 g ZnAl_{0.50}/L

Acknowledgements This project was supported by the Deanship of Scientific Research at Prince Sattam Bin Abdulaziz University under the research project #2015/01/3805.

Compliance with ethical standards

Conflict of interest The authors declare no competing financial interest.

References

- M. Pirhashemi, A. Habibi-Yangjeh, *J. Photochem. Photobiol.* **363**, 31 (2018)
- A. Omo Ibadon, P. Fitzpatrick, *Catalysts* **3**, 189 (2013)
- M. Mousavi, A. Habibi-Yangjeh, S.R. Pouran, *J. Mater. Sci.: Mater. Electron.* **29**, 1719 (2018)
- M. Shekofteh-Gohari, A. Habibi-Yangjeh, *Ceram. Int.* **43**, 3063 (2017)
- M. Pirhashemi, A. Habibi-Yangjeh, *Mater. Chem. Phys.* **214**, 107 (2018)
- M. Pirhashemi, A. Habibi-Yangjeh, *J. Colloid Interface Sci.* **491**, 216 (2017)
- M. Pirhashemi, A. Habibi-Yangjeh, S. Rahim Pouran, *J. Ind. Eng. Chem.* **62**, 1 (2018)
- M. Pirhashemi, A. Habibi-Yangjeh, *Sep. Purif. Technol.* **193**, 69 (2018)
- X.F. Zhao, L. Wang, X. Xu, X.D. Lei, S.L. Xu, F.Z. Zhang, *AIChE J.* **58**, 573 (2012)
- L. Zhang, J. Yana, M. Zhou, Y. Yang, Y. Liu, *Appl. Surf. Sci.* **268**, 237 (2013)
- Z. Li, S. Zhang, W.E. Lee, *J. Eur. Ceram. Soc.* **27**, 3407 (2007)
- L. Zou, F. Li, X. Xiang, D.G. Evans, X. Duan, *Chem. Mater.* **18**, 5852 (2006)
- X. Wei, D. Chen, *Mater. Lett.* **60**, 823 (2006)
- S. Farhadi, S. Panahandehjoo, *Appl. Catal. A* **382**, 293 (2010)
- L. Gama, M.A. Ribeiro, B.S. Barros, R.H.A. Kiminami, I.T. Weber, A.C.F.M. Costa, *J. Alloys Compd.* **483**, 453 (2009)
- L. Chen, X. Sun, Y. Liu, K. Zhou, Y. Li, *J. Alloys Compd.* **376**, 257 (2004)
- Z. Zhu, X. Li, Q. Zhao, S. Liu, X. Hu, G. Chen, *Mater. Lett.* **65**, 194 (2011)
- M. Zawadzki, *Solid State Sci.* **8**, 14 (2006)
- D. Li, Y. Fan, Y. Ding, X. Wei, Y. Xiao, *Catal. Commun.* **88**, 60 (2017)
- X. Li, J. Liu, X. Ji, J. Jiang, R. Ding, Y. Hu, A. Hu, X. Huang, *Sens. Actuators B* **147**, 241 (2010)
- H. Zhang, L. Yina, X. Liu, R. Weng, Y. Wang, Z. Wu, *Appl. Surf. Sci.* **380**, 178 (2016)
- Y. Kuang, L. Zhao, S. Zhang, F. Zhang, M. Dong, S. Xu, *Materials* **3**, 5220 (2010)
- T. Kameda, M. Saito, Y. Umetsu, *Mater. Trans.* **47**, 923 (2006)
- G.B. Sun, L.N. Sun, H. Wen, Z.Q. Jia, K.L. Huang, C.W. Hu, *J. Phys. Chem. B* **110**, 13375 (2006)
- J. Song, M. Leng, X. Fu, J. Liu, *J. Alloys Compd.* **543**, 142 (2012)
- V. Rives, M. Arco, C. Martín, *Appl. Clay Sci.* **88**, 239 (2014)
- J.R. Ebdon, B. Hunt, P.J. Joseph, *Polym. Degrad. Stab.* **83**, 181 (2004)
- S.B. Eshwaran, D. Basu, S.R. Vaikuntam, B. Kutlu, S. Wiessner, A. Das, K. Naskar, G. Heinrich, *J. Appl. Polym. Sci.* **132**, 41539 (2015)
- F.R. Costa, A. Leuteritz, U. Wagenknecht, D. Jehnichen, L. Haußler, G. Heinrich, *Appl. Clay Sci.* **38**, 153 (2007)
- Y. Imai, Y. Inukai, H. Tateyama, *Polym. J.* **35**, 230 (2003)
- P.C. LeBaron, T.J. Pinnavaia, *Chem. Mater.* **13**, 3760 (2001)
- S.S.L. Sobhana, D.R. Bogati, M. Reza, J. Gustafsson, P. Fardim, *Microporous Mesoporous Mater.* **225**, 66 (2016)
- E. Geraud, V. Prevot, F. Leroux, *J. Phys. Chem. Solids* **67**, 903 (2006)
- G. Liu, X. Li, J. Zhao, H. Hidaka, N. Serpone, *Environ. Sci. Technol.* **34**, 3982 (2000)
- G.L. Baughman, E.J. Weber, *Environ. Sci. Technol.* **28**, 267 (1994)
- R. Comparelli, E. Fanizza, M.L. Curri, P.D. Cozzoli, G. Mascolo, A. Agostiano, *Appl. Catal. B* **60**, 1 (2005)
- S. Liao, H. Donggen, D. Yu, Y. Su, G. Yuan, *J. Photochem. Photobiol.* **168**, 7 (2004)
- S.K. Kansal, M. Singh, D. Sud, *J. Hazard. Mater.* **141**, 581 (2007)
- L. Wu, J.C. Yu, X. Fu, *J. Mol. Catal. A* **244**, 25 (2006)
- K. Abderrazek, F.S. Najoua, E. Srasra, *Appl. Clay Sci.* **119**, 229 (2016)
- R. Huo, Y. Kuang, Z. Zhao, F. Zhang, S. Xu, *J. Colloid Interface Sci.* **407**, 17 (2013)
- Y. Guo, D. Li, C. Hu, Y. Wang, E. Wang, Y. Zhou, S. Feng, *Appl. Catal. B* **30**, 337 (2001)
- E.M. Seftel, E. Popovici, M. Mertens, K. DeWitte, G.V. Tendeloo, P. Cool, E.F. Vansant, *Microporous Mesoporous Mater.* **113**, 296 (2008)
- D. Carriazo, M. Del Arco, E. Garcia-Lopez, G. Marci, C. Martin, L. Palmisano, V. Rives, *J. Mol. Catal. A* **342**, 83 (2011)
- S. Milica, J.H. Tatjana, B.V. Dmitar, P.Z. Radmila, M. Nedučin, *Chem. Ind. Chem. Eng. Q.* **18**, 295 (2012)
- D. Meloni, R. Monaci, V. Solinas, A. Auroux, E. Dumitriu, *Appl. Catal. A* **350**, 86 (2008)
- H. Cui, Y. Zhou, J. Mei, Z. Li, S. Xu, C. Yao, *J. Phys. Chem. Solids* **112**, 80 (2018)